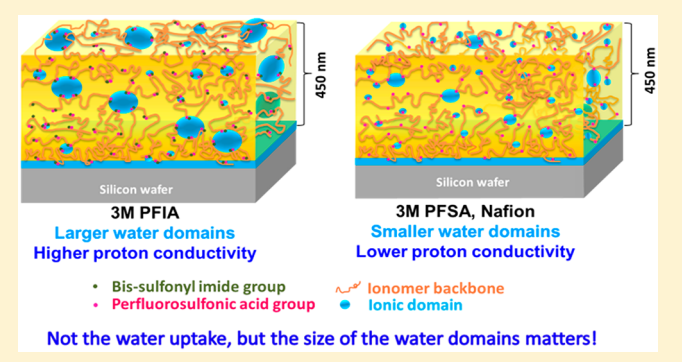
Fluorocarbon-Based Ionomers with Single Acid and Multiacid Side **Chains at Nanothin Interfaces**

Seefat Farzin, Anandakumar Sarella, Michael A. Yandrasits, and Shudipto K. Dishari

Supporting Information

ABSTRACT: Unraveling ion conduction limitations in nanothin ionomer films is crucial for designing efficient ionomer-catalyst interfaces and improving redox efficiency in electrochemical devices. This work took a multifaceted approach to understand local proton conduction environments in sub-µm thick films of three fluorocarbon-based ionomers, Nafion, 3M PFSA and 3M PFIA with IEC ~ 0.91, 1.21, and 1.61 mequiv/g, respectively. After incorporating fluorescent photoacid probe pyranine (HPTS) into films, the extent of proton conduction (I_d/I_p) , local proton concentration, pH, and ionic domain size (d_{id}) were predicted by monitoring the ratio of fluorescence intensity of deprotonated $(I_{\rm d})$ to that of the protonated $(I_{\rm p})$ state of HPTS. $I_{\rm d}/I_{\rm p}$



decreased with film thickness and followed the trend: 3M PFIA > 3M PFSA > Nafion. A higher water uptake did not necessarily lead to higher I_d/I_p indicating that other factors than water uptake control proton conduction under confinement. Size of the ionic domains (d_{id}) , measured independently using in-plane reflection small-angle X-ray scattering and fluorescence spectroscopy, followed the same trend as $I_{\rm d}/I_{\rm p}$. As the RH and film thickness decreased, $d_{\rm id}$ became smaller. The close match of d_{id} obtained from both techniques supported the reliability of information confered by fluorescence spectroscopy about key controlling parameters of the local proton conduction environment. The highest $I_{\rm d}/I_{\rm p}$ of 3M PFIA films was attributed to its flexible, multiacidic side chain that helped to form larger ionic domains with better phase segregation. Conversely, smaller, extremely acidic and poorly phase segregated ionic domains with highly confined water molecules led to lower I_d/I_p in Nafion films, despite high water uptake.

■ INTRODUCTION

The behavior of polymers in sub-µm thick films can be drastically different from that in bulk membrane format (several tens of μ m thick). Polymer chains experience confinement within films when the film thickness approaches the radius of gyration of free polymer chains. 1-3 The polymer chain entrapment as well as complex interfacial interactions (among water, polymer, and substrate) impacts the rheology^{4–8} and diffusion coefficient of both water and polymer chains^{9–12} in hydrated thin films. These can make the watermediated ion conduction very difficult in thin films of ion conducting polymer (ionomer), 13-17 critical for energy technologies. Factors, such as chemical structure of ionomers ¹³, ¹⁵, ¹⁸⁻²⁰ ionomer film thickness, ¹³, ¹⁵, ¹⁸⁻²¹ film casting method, ¹⁶, ¹⁸, ²², ²³ pretreatment procedure, ²², ²⁴⁻²⁷ and nature of the substrate, ²⁸, ²⁹ can lead to substantial changes in nanostructure, ¹³, ²³, ²² water uptake, ¹⁸, ²³ water—ionomer distribution, ^{28,19,21,29} mechanical properties, ^{18,22} and ion conduction properties 13,16,23,30,31 of sub- μ m thick ionomer films. Since ion conduction under nanoconfinement is a complex

outcome of multiple phenomena, we need deeper insights into the local hydration and ion conduction environment within sub-µm thick, supported ionomer films to better understand ion conduction at nanothin (~2-30 nm thick) ionomercatalyst interfaces. Such work can help to set design rules for next-generation ionomer-based catalyst binders for energy conversion and storage devices (such as proton exchange membrane fuel cells, electrolyzers, and redox flow batteries).

Nafion, the current state-of-the-art fuel cell ionomer, consists of a fluorocarbon-based backbone with primary and secondary side chains (Figure 1, left). The perfluorosulfonic acid groups at the end of primary side chains dissociate to give counterions (H⁺) and are responsible for proton conduction. Nafion efficiently conducts protons $(\sim 50-100~mS/cm)^{32,33}$ in bulk membranes (\sim 25–50 μ m thick) due to efficient phase separation and formation of wide and interconnected ion

Received: October 24, 2019 Revised: November 26, 2019 Published: December 2, 2019

Department of Chemical and Biomolecular Engineering, University of Nebraska—Lincoln, Lincoln, Nebraska 68588, United States *Nebraska Center for Materials and Nanoscience, Voelte-Keegan Nanoscience Research Center, University of Nebraska—Lincoln, Lincoln, Nebraska 68588-0298, United States

 $^{^{\}perp}$ 3M Fuel Cell Components Program, 3M Company, St. Paul, Minnesota 55144, United States

Figure 1. Chemical structures of Nafion, 3M PFSA, and 3M PFIA.

channels (~4 nm) within the membrane. 34,35 However, the proton conductivity of Nafion in sub- μ m thick films is low ^{13,14} (\sim 3.8 mS/cm for 10 nm thick annealed, self-assembled film³⁰). The significantly higher activation energy of proton conduction was reported for a 50 nm thick self-assembled Nafion film as compared to a 50 μ m thick bulk Nafion membrane³⁶ supporting limited proton conduction in sub- μ m thick Nafion films. The interfacial attractive interactions (such as hydrogen bonding among water, ionomer, and substrate) 15 became more pronounced in supported, Nafion thin films and led to a nonhomogeneous distribution of water across the films (e.g., segregation near substrate interface), ^{28,37,38} and hydration induced film stiffening. ^{18,19} These interfacial interactions and film stiffening limited the water and proton mobility as the ionomer films became thinner. Also, the slow proton transport dynamics^{39,40} was associated with low rotational mobility⁴¹ and slow orientation relaxation dynamics of water 42 since efficient proton hopping requires water molecules to continuously rotate, break, and form hydrogen bonds with neighboring water molecules. Moreover, distinctly different phase separation and ionic domain size were predicted for bulk membrane and thin films of Nafion. 23,34 Under thin film confinement, the spontaneous self-assembly of ionomers was restricted resulting in small ionic domains²³ with a higher degree of phase mixing.²³ In addition, low pH, very high proton concentration in such small ionic domains shifted the proton transport dynamics backward making a dominant population of the protonated form of the sulfonic acid groups of the ionomer chains. ^{15,42} These thin film studies, however, focused mostly on Nafion, ^{13,15,18,43} with a little on S-Radel, ^{19,44} and a few other ionomers. ^{20,21}

In order to achieve proton conductivity and durability superior to Nafion, a number of fluorocarbon⁴⁵ and hydrocarbon 46-48 based new ionomer design efforts have been made. The current work focused on understanding the local hydration/proton conduction environment and its connection with water uptake, ionic domain characteristics and morphology of three fluorocarbon-based, potential fuel cell ionomers, Nafion (Figure 1, left), 3M PFSA^{49,45,50} (Figure 1, middle), and 3M PFIA (Figure 1, right). 3M PFSA and 3M PFIA were chosen for this study as bulk membranes (\sim 25 μ m thick) of both 3M PFSA and 3M PFIA showed proton conductivity better than Nafion. 13,49,51 While all three ionomers have a

fluorocarbon-based backbone, their side-chain chemistries are different. 3M PFSA has fluorocarbon-based primary side chains having a perfluoroether group and one perfluorosulfonic acid (-CF₂SO₃H) group per side chain. On the other hand, Nafion has both primary and secondary side chains, 2 perfluoroether groups, and, one perfluorosulfonic acid (-CF₂SO₃H) group per side chain. While Nafion and 3M PFSA have a single acid group (-CF₂SO₃H) per side chain, 3M PFIA has multiple acid groups per side chain: a highly protogenic perfluorobis-(sulfonyl) imide (R_FSO₂-NH-SO₂-R_f) group, in addition to perfluorosulfonic acid (-CF₂SO₃H). The strong electronwithdrawing nature of the neighboring -CF₂- groups, as well as sulfone (-SO₂-) groups of bis(sulfonyl) imide (-SO₂-NH-SO₂-) moieties make the proton dissociation from -NH- facile and the polymer PFIA extremely acidic. 45,52,53 Moreover, the presence of multiple acid groups per side chain helped 3M PFIA to achieve high ion exchange capacity (IEC = milliequivalent of acid group/g of polymer). 45,54 In the bulk membrane format (\sim 25 μ m thick), both 3M PFSA and 3M PFIA exhibited proton conductivity better than Nafion.

In this work, we leveraged a fluorescent photoacid probe, HPTS that fluorescently responded to local hydration environment when incorporated within sub- μ m thick (~20-470 nm thick) films of Nafion (EW ~ 1100, IEC = 0.909 mequiv/g), 3M PFSA (EW \sim 825, IEC = 1.21 mequiv/g), and 3M PFIA (EW \sim 620, IEC = 1.61 mequiv/g) exposed to air with certain relative humidity (RH). Fluorescent dyes have been found effective to reveal the glass transition, 7,6,55,56,5 water sorption and diffusivity, ^{10,57,58} aging ^{6,56,59} or structural relaxation, ⁶⁰ polymer—substrate interaction, ^{15,59} proton conduction, ¹⁵ and mechanical behavior ^{18,19,58} within confined systems. Many critical parameters of proton conduction environment, such as the extent of proton conduction, 15,61 proton transport dynamics, 11,12,39,40 and water orientational relaxation dynamics 42 have been investigated by incorporating photoacid probes within polymeric, ^{11,12,15,39,42,61} reverse micelle, ^{11,12,39,62,63} and biological ^{64,65} systems. The extent of proton conduction in these systems is represented by the term deprotonation ratio (I_d/I_p) of a photoacid probe, 8hydroxypyrene-1,3,6 trisulfonic acid sodium salt or pyranine (HPTS, see Figure 2 for working principle).

When the deprotonation ratio (I_d/I_p) and quantitative values of proton conductivity (σ) at similar hydration

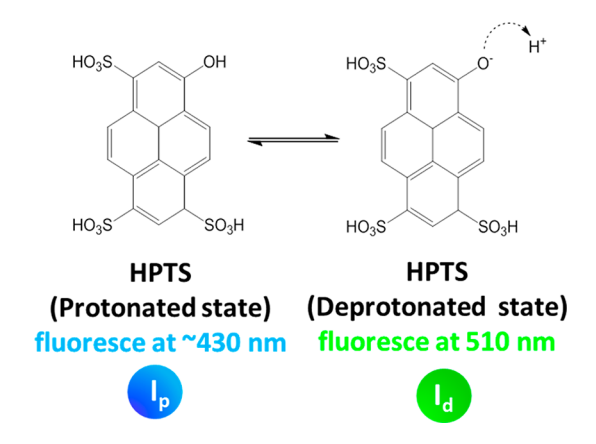


Figure 2. Working principle of photoacid probe HPTS. The dye stays protonated (R–OH) at the dry state or in a poorly proton-conducting environment. The protonated state of HPTS gives blue fluorescence with an emission peak at a wavelength (λ) of ~425–450 nm (denoted by $I_{\rm p}$). On the other hand, HPTS, just like any ionomer, donates its phenolic proton (R–OH \rightarrow R–O $^-$ + H $^+$) if the surrounding hydration environment is favorable to accept and conduct proton from its generation site. ^{15,61} The deprotonated state emission of HPTS is denoted by $I_{\rm d}$ and emits green fluorescence (λ ~ 510 nm). The deprotonation ratio ($I_{\rm d}/I_{\rm p}$) is considered as the extent of proton transfer which offers information complementary to the quantitative value of proton conductivity (σ).

numbers $(\lambda_{\rm w})$ were plotted for bulk Nafion membrane, an almost linear trend was seen (Figure S1). $I_{\rm d}/I_{\rm p}$ and σ thus offer complementary information. The added advantage of using HPTS is that the dye helps to extract some of the critical information (in addition to $I_{\rm d}/I_{\rm p}$) about the local hydration environment, such as pH, local proton concentration, and ionic domain size which work together to give rise to certain quantitative values of proton conductivity (σ) (reported often using electrochemical impedance spectroscopy). Dishari and Hickner showed earlier that thin films of Nafion experience a lower extent of proton transfer $(I_{\rm d}/I_{\rm p})$ as compared to bulk Nafion membrane. Moreover, HPTS was able to distinguish between the proton conduction behavior in nanoscopic water and bulk water in Nafion thin films and membranes, an advantage of the spectively.

In this work, the extent of proton conduction (I_d/I_p) of HPTS incorporated in sub- μ m thick films of 3M PFIA, 3M PFSA, and Nafion as a function of film thickness, and relative humidity was studied. We predicted the diameter of ionic domains (d_{id}) within ionomer films by comparing the deprotonation ratio (I_d/I_p) of ionomer films to that of AOT reverse micelle systems with the known size of nanoscopic water core. The values of d_{id} for the three ionomers at the varied thickness and relative humidity were further verified using another independent technique, in-plane reflection smallangle X-ray scattering (RSAXS). RSAXS revealed the ionic domain spacing (d-spacing = $2\pi/q_{\rm p,max}$) where $q_{\rm p}$ corresponding to the ionic domain spans between 1.5 and 3.5 nm⁻¹). In addition, a subsequent least-squares fit of the ionic domain peaks using in Nanosolver^{67,68} (a built-in software of Rigaku Smartlab Diffractometer) gave the average size of ionic domains (d_{id}) in all ionomer films at dry and humid conditions, where the experimentally calculated d-spacing for a film was used as an input parameter. By analyzing the nanoscale morphology (of the dry ionomer films using brightfield transmission electron microscopy), water uptake (λ_{wt}

quartz crystal microbalance), pH (fluorescence), proton concentration (fluorescence), and ionic domain size (fluorescence, RSAXS) within ionomer films, we rationalized the observed extent of proton conduction ($I_{\rm d}/I_{\rm p}$) in sub- μ m thick ionomer films, and evaluated the most important parameters impacting the proton conduction under nanoconfinement. For all the measurements, we used a consistent film preparation technique (films were spin-coated on the native oxide of SiO₂ (n- SiO₂) based substrates and annealed) to more accurately correlate the thin film ionomer properties. Also please note that the term "extent of proton conduction" was used throughout this paper to indicate the values of $I_{\rm d}/I_{\rm p}$ and distinguish from the quantitative values of proton conductivity (σ), measured typically using electrochemical impedance spectroscopy.

■ EXPERIMENTAL SECTION

Materials. HPTS dye was purchased from Fisher Scientific (Somerville, NJ). A 20 wt % Nafion solution (EW \sim 1100, IEC 0.909 mequiv/g) was purchased from Sigma-Aldrich (Milwaukee, WI). 3M PFIA (EW \sim 620, IEC 1.61 mequiv/g) and 3M PFSA (EW \sim 825, IEC 1.21 mequiv/g) ionomer powders were generously provided by 3M Inc. (St. Paul, MN). Ethanol and acetone were purchased from Fisher Scientific (Hampton, NH). Silicon wafers coated with native silicon dioxide (n-SiO $_2$ wafers) were purchased from Wafer Pro (San Jose, CA), and 0.2 μ m syringe filters were purchased from VWR (Radnor, PA).

Thin Film Preparation. A 20 wt % Nafion solution was diluted with ethanol from 10 wt % to 0.5 wt % to yield 470 to 20 nm thick films. 3M PFIA and 3M PFSA ionomer powders were dissolved into pure ethanol and ethanol/water (3:1) mixture, respectively followed by filtration with 0.2 μ m syringe filters to prepare ionomer solutions at certain wt % to yield films with a thickness similar to Nafion films. A stock solution of HPTS in DI water was then added into these polymers solutions to yield a final dye concentration of 0.75 mM in ionomer solutions. n-SiO2 wafers were cut into small pieces (2 $cm \times 2.5$ cm) to use as substrates for making ionomer films. After removing dust particles using compressed air, the substrates were (i) rinsed with acetone and ethanol, (ii) dried with compressed air, and (iii) UV-ozone treated subsequently to clean the surface. The films were then spincoated using an EC 101 spin coater (Headway Research, Inc., Garland, TX) for 40 s at 3000 rpm. The films were placed in a vacuum oven (Model # 1415 M, VWR, Radnor, PA), dried at 42 °C for 3 h, annealed at 100 °C for 7 h and cooled down to room temperature for 12 h under vacuum. The films were then placed inside an appropriate humidity chamber and exposed to air with varied relative humidity (RH) for measurements.

Fluorescence Spectroscopic Measurement. Steady-state fluorescence spectra of ionomer thin films on n-SiO $_2$ wafers were taken using fluorescence spectroscopy (PTI Quantamaster 400, Horiba, NJ). The excitation wavelength of HPTS was 370 nm, and the emission wavelengths for HPTS ranged from 390 to 590 nm. Fluorescence data of all samples were obtained using the same spectroscopic parameters (excitation/emission slit width = 1 nm; step size = 10 under excitation correction and zero bias). A custom-built glass humidity chamber (2.25 in. \times 2.25 in. \times 2.875 in.) was used for relative humidity (RH) based fluorescence measurements. The RH of air was controlled using a humidifying system (ibidi USA, Inc., Fitchburg, WI).

Water Uptake Measurement. The measurement of water uptake was performed using quartz crystal microbalance (QCM) (Stanford Research Systems, Sunnyvale, CA). Ionomer films (without HPTS) were spin-coated on n-SiO₂/Au coated 5 MHz crystals (Inficon, Syracuse, NY) and annealed following the procedure mentioned before. The humidity inside a custom-built plastic humidity chamber was controlled using the same ibidi humidifying system (mentioned earlier). The total mass of absorbed water (Δm) was calculated using the Sauerbrey equation from the change in frequency (Δf) of ionomer films on QCM crystals due to mass adsorption upon exposure to humid air:

$$\Delta f = -\frac{2f_0^2 \Delta m}{A\sqrt{\rho_q \mu_q}} \tag{1}$$

Here f_0 is the resonant frequency (Hz) of the fundamental mode of the crystal, A is the active crystal area (0.402 cm²), ρ_{q} is the density of quartz crystal (2.648 g/cm³), and $\mu_{\rm q}$ is the shear modulus of quartz (2.947 × 10¹¹ g/cm·s²). The mass of ionomer absorbed on QCM crystal was calculated based on the difference between frequency (Δf) of the bare crystal and dry ionomer film on the crystal. On the other hand, the mass of water uptake at each RH was calculated from the frequency difference between dry film and humidified film on QCM crystal at certain RH. Since water accumulation within the porous structure of the QCM crystals was evidenced earlier, $^{69-71}$ the mass of water uptake (Δm) was corrected by subtracting the amount of water sorbed by bare, annealed QCM crystal from the water mass sorbed by individual ionomer films. This procedure gave the corrected mass of water adsorbed only inside the ionomer films. The mass of water uptake (Δm) was then converted into hydration number, λ_{wt} defined by moles of water per mole of proton conducting groups using the following equation:

$$\lambda_{w} = \left(\frac{m_{\text{RH}} - m_{0}}{M_{\text{H}_{2}\text{O}}}\right) \left(\frac{1000}{m_{0} \times \text{IEC}}\right) \tag{2}$$

Here $m_{\rm RH}$ is the sample mass at a certain RH, m_0 is the mass of the dry sample, $M_{\rm H_2O}$ is the molecular mass of water, and IEC is the ion-exchange capacity.

Thickness Measurement. The thickness of ionomer films was measured at ambient conditions using variable angle (65–75°) spectroscopic ellipsometry (α -SE, J.A. Woollam Co., Inc., Lincoln, NE) with a spectral wavelength range of 381–893 nm. The thickness of the native oxide layer on a silicon wafer (\sim 1.77 nm), measured before measuring the thickness of ionomer films, was used as a reference for ellipsometric modeling. The Cauchy model was used to obtain the thickness of all the ionomer films.

In-Plane Reflection Small-Angle X-ray Scattering (RSAXS) Measurement. To investigate the morphological information, RSAXS measurements were performed at ambient conditions using a Rigaku Smartlab Diffractometer operating at 40 kV and 44 mA using a sealed Cu anode X-ray tube with an average wavelength (λ^*) of 1.5418 Å. Conventionally, grazing incidence small-angle X-ray scattering (GISAXS) is performed for the nanostructure determination of thin films using a 2D detector. While the 2D detector has the advantage of simultaneously measuring intensities in both in-plane (q_p) and out of plane (q_z) directions (and hence resolving the lateral and vertical correlation lengths), our SAXS system used

a 0 D approach (point detector), where only one of these components was resolved dependent on the type of scan chosen.⁷² This is, in fact, a special case of grazing incidence SAXS (GISAXS) technique, more specifically called reflection SAXS (RSAXS), where we used grazing incidence illumination of the sample, but captured the off-specular reflection signals using a point detector. In RSAXS, the data were collected in asymmetric $\omega/2\theta$ geometry (i.e., $\omega \neq \theta$, where ω and 2θ are incident and scattering angles, respectively). In this case, the scan was performed by intentionally offsetting ω by an appropriate angle to avoid specular reflection (in specular reflection, $\theta_i = \theta_{fi}$ where θ_i and θ_f are the incidence and exit angles, respectively) signal and capture the off-specular scattering (where $\theta_i \neq \theta_f$) signal.⁷³ The scattered beams were scanned in the angular range (2θ) of 0 to 6° with a step size of 0.02°. With this off-specular scattering, the lateral component (q_p) was obtained which provided the in-plane structure of the sample.⁷⁴ Thin films (without HPTS) with thickness in the range of 20-450 nm, deposited on n-SiO₂ wafers with native oxide, were placed on a sample holder disc and optically aligned. The distance between the sample and the detector was 30 cm. The in-plane scattering vector, q_p is directly related to its scattering angle, 2θ (the angle between the incident beam and scattered beam) and X-ray wavelength,

$$q_{\rm p} = \frac{4\pi}{\lambda^*} \sin(\theta) \tag{3}$$

The domain spacing for ionic domains (d) within the films was determined based on their primary scattering peak maxima, $q_{\rm p,max}$ in their specified region $(1.50-3.50~{\rm nm}^{-1})$ using

$$d = \frac{2\pi}{q_{\text{p,max}}} \tag{4}$$

In addition to the measurement at an ambient relative humidity (~56% RH), RSAXS patterns were obtained at 90% RH. Since a setup for continuous, external humid airflow during measurement was not available for the RSAXS instrument, annealed ionomer films were exposed to air with 90% RH at room temperature in an external humidity chamber overnight prior to RSAXS measurement. The samples were then carried in an enclosed container carefully to the RSAXS facility. A custom-built plastic container with a traceable humidity sensor (Fisher Scientific, Hampton, NH) was used for in situ monitoring the humidity within the sample chamber of RSAXS. Two windows $(2 \text{ cm} \times 2 \text{ cm})$ were cut in the plastic container and sealed with Chemplex SpectroFilm (Palm City, FL) provided by the RSAXS facility to allow passage of X-ray and maintain the humidity. Inside the plastic container, 2-3 small beakers (5 mL) with warm water were kept to reach 90% RH (confirmed using the traceable humidity sensor inserted). The schematic of humidity setup (Figure S2) and the details of fitting of RSAXS data are shown in Supporting Information.

Bright-Field Transmission Electron Microscope (TEM) Imaging. For the investigation of the morphology of ionomer films with thickness <100 nm, a 40 nm thick silicon dioxide support layer (Ted Pella, Inc., Redding, CA) on SiO₂ grid was used as a substrate. Polymer solutions without HPTS were directly dispensed onto that grid with SiO₂ support layer and spin-coated to yield 20–75 nm thick ionomer films. The films were annealed using the same protocol stated before. Bright-

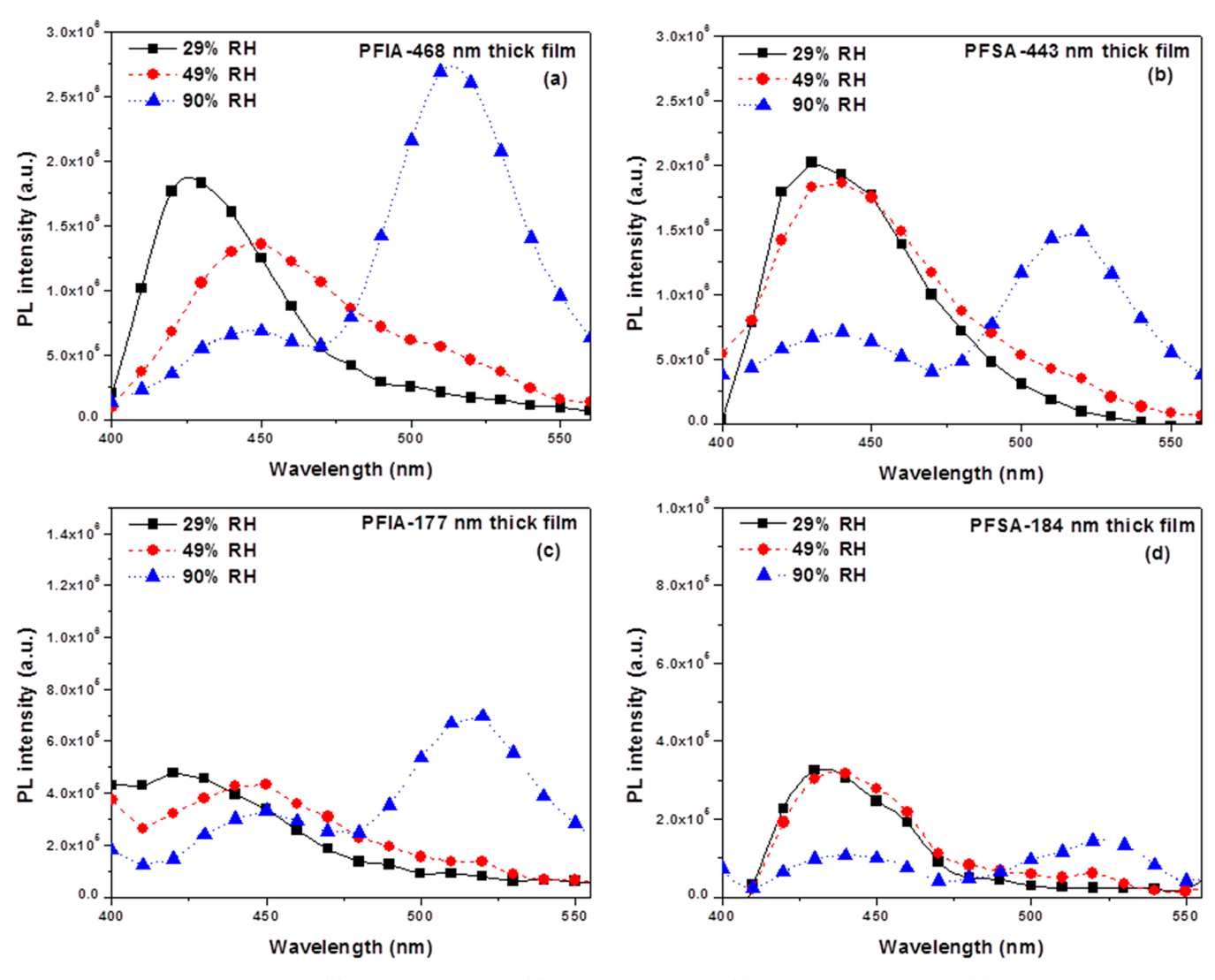


Figure 3. Fluorescence response of (a) 468 nm 3M PFIA; (b) 443 nm 3M PFSA; (c) 177 nm 3M PFIA, and (d) 184 nm 3M PFSA films containing HPTS (λ_{ex} 370 nm and λ_{em} 390–590 nm). All the films were spin-coated on the n-SiO₂ substrates and annealed.

field TEM images were acquired using a FEI Tecnai Osiris (Scanning) transmission electron microscope operated at 200 kV

RESULTS AND DISCUSSIONS

Fluorescence-Based Measurement of the Extent of Proton Conduction. Fluorescent photoacid probe HPTS (Figure 2) was incorporated into ~170-470 nm thick films of 3M PFIA (Figure 3a,c), 3M PFSA (Figure 3b,d), and Nafion (as discussed in the Experimental Section), and exposed to humid air (~29-90% RH) to probe the extent of proton conduction $(I_d/I_p$, Figure 4) and parameters of local hydration environment (pH, proton concentration, ionic domain size, discussed later) within ionomer films. As discussed earlier, the protogenic behavior of HPTS is similar to that of the ionomers at dry and hydrated states. Thus, the higher the emission of deprotonated state of HPTS (I_d , $\lambda_{em,max}$ at ~515 nm) relative to that of protonated state ($I_{\rm p}$, $\lambda_{\rm em,max} \sim 425-450$ nm), the higher the value of deprotonation ratio (I_d/I_p) and the extent of proton conduction is. A negligible or less pronounced I_d peak was observed in steady-state fluorescence spectra of all ionomer films up to 50% RH. A significant rise of I_d was seen at 90% RH, indicating significant deprotonation of HPTS and

an increase in proton conduction in ionomer films at higher RH. The red shift of protonated peak in some cases could be attributed to the changes in local polarity around the dye molecules while the films were hydrated gradually. The 468 nm thick 3M PFIA film showed the highest emission at 510 nm $(I_{\rm d})$ out of the films of all ionomers at a similar thickness (Figure 3a).

The deprotonation ratio (I_d/I_p) of 468 nm thick 3M PFIA film (Figure 4a) was 5 times higher than a Nafion film (Figure 4b) and ~2 times higher than a 3M PFSA film (Figure 4c) with similar thickness. The extent of proton conduction (or I_d/I_p) for the three ionomers consistently followed the trend: 3M PFIA> 3M PFSA > Nafion at similar film thickness (Figure 4). Since the three ionomers we studied have different IECs, we normalized the values of I_d/I_p with respect to IECs of corresponding ionomers $((I_d/I_p)/\text{IEC})$. The IEC normalized I_d/I_p (Figure 4d) also showed the same trend: 3M PFIA> 3M PFSA> Nafion at similar thickness at 90% RH. The observed trends in the extent of proton conduction for sub- μ m thick films were in agreement with that in membrane 45,49,52 format for these ionomers. The Gibbs free energy of acid dissociation (also termed as gas-phase acidity) of bis sulfonyl imide group $(\Delta G_{acid} = 284.1 \text{ kcal/mol})^{76}$ present only in 3M PFIA is lower

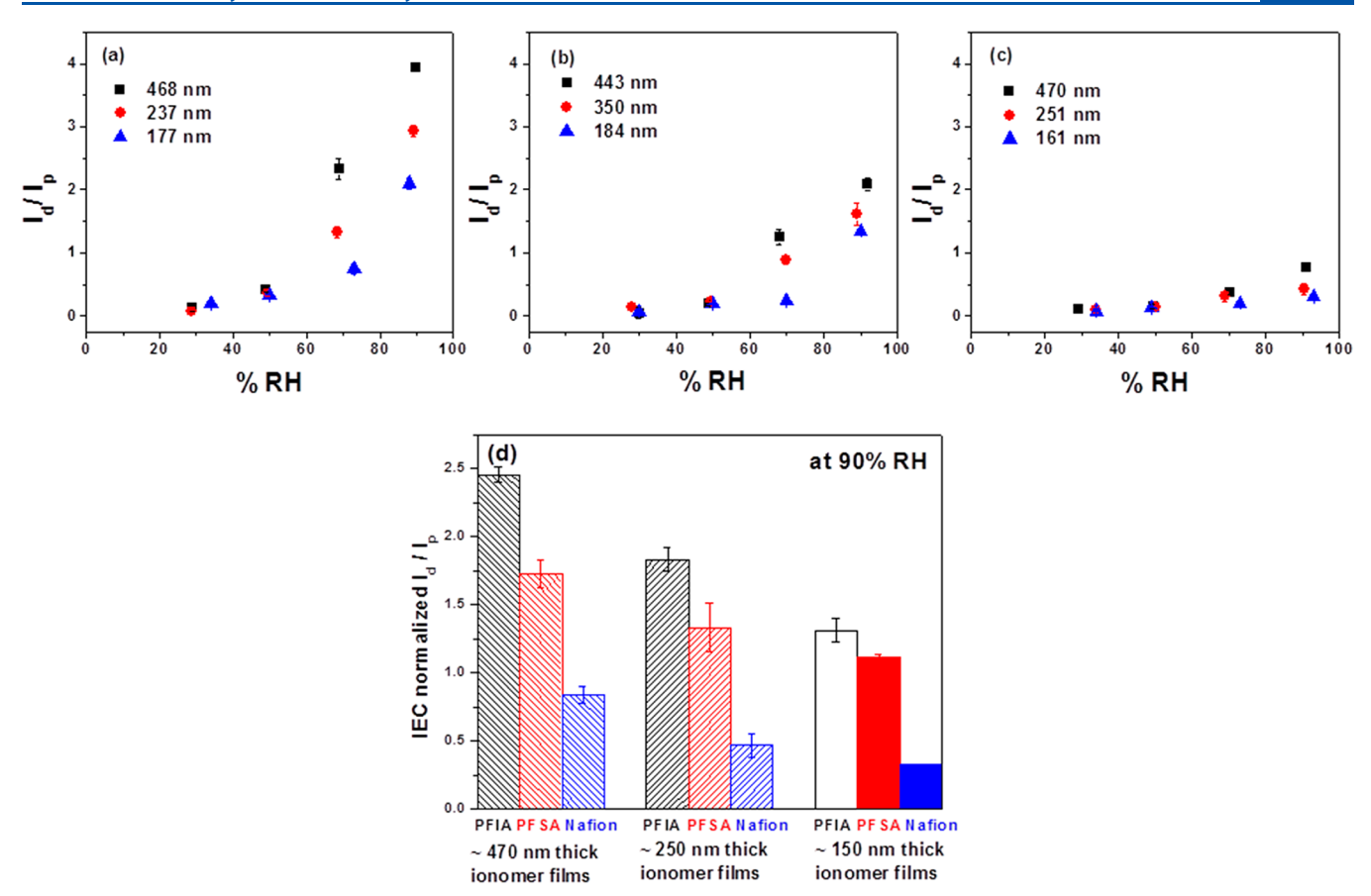


Figure 4. Ratio of fluorescence intensities of deprotonated (I_d) to protonated (I_p) state of HPTS, (I_d/I_p) , with precision error bars) in (a) 3M PFIA, (b) 3M PFSA, and (c) Nafion ionomers on n-SiO₂ substrate at different RH as a function of film thickness. IEC normalized I_d/I_p (i.e., (I_d/I_p) /IEC) (with precision error bars) of all ionomer samples at 90% RH (d).

Table 1. pH and Proton Concentration (Average) of Ionic Domains within Ionomer Films as a Function of Film Thickness and RH

		$I_{ m d}/I_{ m p}$		local pH ^a of ionic domains		$\begin{array}{c} \text{local proton concentration } [H^+] \text{ in} \\ \text{ionic domains } (M) \end{array}$	
polymer	sample thickness (nm)	56% RH	90% RH	56% RH	90% RH	56% RH	90% RH
3M PFIA	468	0.37 ± 0.04	3.88 ± 0.05	0.14 ± 0.07	2.27 ± 0.34	0.74 ± 0.12	0.01 ± 0.005
	237	0.36 ± 0.05	2.84 ± 0.09	0.14 ± 0.09	2.27 ± 0.34	0.75 ± 0.16	0.01 ± 0.005
	177	0.34 ± 0.02	2.02 ± 0.08	0.08 ± 0.04	1.77 ± 0.16	0.84 ± 0.08	0.02 ± 0.007
3M PFSA	443	0.20 ± 0.02	1.99 ± 0.10	-0.72 ± 0.12	1.75 ± 0.18	6.00 ± 1.00	0.02 ± 0.008
	350	0.23 ± 0.01	1.44 ± 0.17	-0.70 ± 0.00	1.31 ± 0.12	5.00 ± 0.00	0.05 ± 0.013
	184	0.22 ± 0.01	1.33 ± 0.02	-0.70 ± 0.00	1.21 ± 0.02	5.00 ± 0.00	$0.06 \pm 0.0.003$
Nafion	470	0.11 ± 0.03	0.70 ± 0.06	-1.00 ± 0.00	0.59 ± 0.04	10.00 ± 0.00	0.26 ± 0.025
	251	0.17 ± 0.03	0.51 ± 0.09	-1.00 ± 0.00	0.29 ± 0.06	10.00 ± 0.00	0.53 ± 0.065
	161	0.09 ± 0.04	0.29 ± 0.01	-1.00 ± 0.00	0.00 ± 0.00	10.00 ± 0.00	1.00 ± 0.000

^aHCl solutions at different concentrations were prepared and pH values were measured first. The fluorescent dye HPTS (15 μ M) was then added to each acid solution to obtain fluorescence response (I_d/I_p) of the dye as a function of pH. The negative pH values were simply calculated using the equation: pH = $-\log_{10}[H+]$, since the pH meter is not suitable to accurately measure negative values of pH.

than perfluorosulfonic acid ($\Delta G_{\rm acid} = 299.5 \, \rm kcal/mol)$, ⁷⁶ present in Nafion, 3M PFSA, and 3M PFIA. Due to the extremely acidic behavior of the bis sulfonyl imide group, 3M PFIA showed the strongest proton conduction behavior even under thin film confinement. However, the less favorable proton conduction environment in thinner films (as seen from the decreasing $I_{\rm d}/I_{\rm p}$ values, Figure 4), maybe a result of multiple factors impacting proton conduction, broadly, water—ionomer confinement, film hydration level, and ionic domain

characteristics. In this work, we put efforts to understand the individual roles of each of these different factors.

The proton concentration ($[H^+]$) and pH of ionic domains within ionomer films, on an average, were predicted by comparing the deprotonation ratio (I_d/I_p) of ionomer films (Figure 4) to that of HPTS in solution (Figure S3). The results are summarized in Table 1. As the film thickness and RH decreased, a decrease in the extent of proton conduction (i.e., decrease in I_d/I_p) and pH of ionic domains; while an increase in proton concentration ($[H^+]$) in the ionic domain were

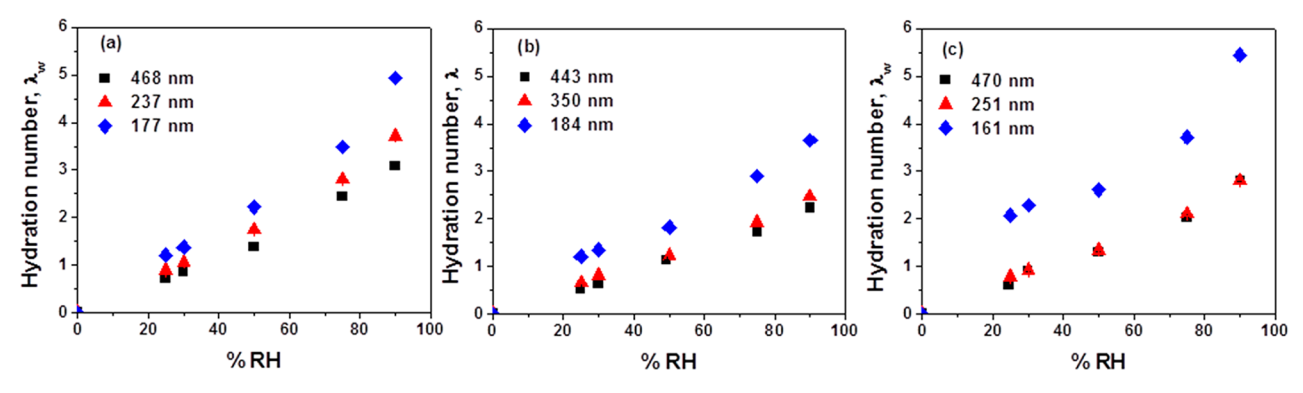


Figure 5. Hydration numbers (λ_w) (bare crystal water sorption corrected and with precision error bars) as a function of RH for (a) 3M PFIA, (b) 3M PFSA, and (c) Nafion ionomers deposited on SiO₂/Au crystal.

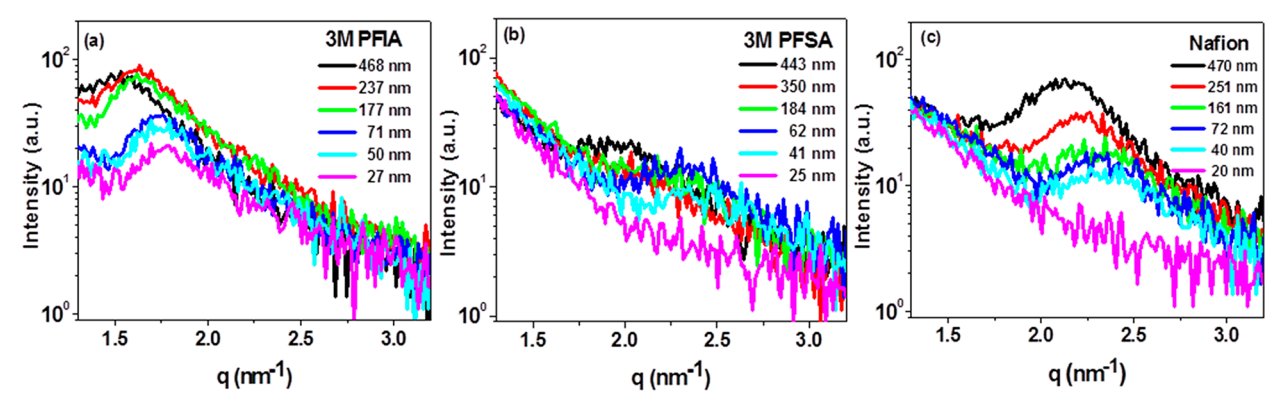


Figure 6. RSAXS patterns (line profiles) of annealed (a) 3M PFIA, (b) 3M PFSA, and (c) Nafion films on the n-SiO₂ wafer as a function of film thickness at ambient condition (\sim 56% RH).

observed. A Nafion film ($[H^+] \sim 2 \text{ M}$) and 3M PFSA ($[H^+] =$ 60 mM) film with thicknesses ~175 nm conducted protons less efficiently (as per I_d/I_p) than a 3M PFIA film ([H⁺] = 12-22 mM) with similar thickness. An extremely acidic pH and high proton concentration ([H+]) can be the results of protonic confinement within an ionic domain and a very slow relay of protons to neighboring ionic domains. 42,61 Ion conductivity is known to be functions of both ion concentration and ion mobility. Thus, even if the proton concentration is high, proton conduction can be weak if the protons are not mobile. Moreover, the proton transfer dynamics studies suggest that when the acidity becomes very high in confined ionic domains, the equilibrium of the proton dissociation reaction tends to shift toward geminate recombination (where dissociated proton reassociates with conjugate anion),⁴² making the proton dissociation and conduction far more difficult.

Water Uptake. Hydration numbers ($\lambda_{\rm w}$ = moles of water/mol of proton conducting groups) of ionomer thin films, calculated from QCM data are plotted as a function of RH (Figure 5). Hydration number (λ) increased with the increase in RH and followed the trend: Nafion > 3M PFIA > 3M PFSA. IEC of individual ionomers may not be solely controlling the hydration as Nafion has the lowest IEC (\sim 0.91) of all three ionomers, but exhibits the highest hydration number ($\lambda_{\rm w}$) in \sim 161 nm thick films. The higher water sorption of Nafion (IEC \sim 0.91) over 3M PFSA (IEC \sim 1.21) could be attributed to the presence of extra perfluoroether group at the side chain in Nafion which offered higher side-chain polarity and flexibility⁷⁷ to Nafion chains. Despite having the highest IEC, 3M PFIA (IEC \sim 1.61) showed water uptake intermediate

between Nafion and 3M PFSA and is likely due to a balance between two structural aspects: (a) longer fluorocarbon sidechain imparting hydrophobicity; (b) 4 oxygen atoms present in bis(sulfonyl imide) $(-SO_2-NH-SO_2-)$ group imparting polarity to side chains.

Most notably, there was no straightforward correlation between hydration number (λ_w , Figure 5) and the extent of proton conduction $(I_d/I_p, Figure 4)$. The λ_w value of 3M PFIA film (\sim 4.94) was intermediate between 3M PFSA (\sim 3.65) and Nafion (\sim 5.46) films when film thickness was \sim 160 nm (Figure 5). However, the 3M PFIA film showed the highest I_d / $I_{\rm p}$ of all 3 ionomers ($(I_{\rm d}/I_{\rm p})_{\rm PFIA}$ = 2.09, $(I_{\rm d}/I_{\rm p})_{\rm PFSA}$ = 1.33, and $(I_{\rm d}/I_{\rm p})_{\rm Nafion}$ = 0.29, Figure 4). The answer to why 3M PFIA needed less water than Nafion to conduct proton in thin films may be complicated and not so straightforward. The 160 nm thick Nafion sample, on the other hand, showed the lowest extent of proton conduction (lowest $I_{\rm d}/I_{\rm p}$) despite having the highest hydration number among all the polymers. Not only that, the thinner films showed higher λ_w (Figure 5) but lower $I_{\rm d}/I_{\rm p}$ values (Figure 4). Typically, it is expected that with the increase in λ_w , proton conduction will improve. These observations were thus counterintuitive but consistent with prior reports on Nafion films. 15,15,22 A 70 nm thick Nafion film showed hydration number similar to a 50 μ m thick Nafion bulk membrane. 15 However, the $I_{\rm d}/I_{\rm p}$ value was an order of magnitude lower in the thin film as compared to the bulk membrane. 15 All these facts indicate that there are factors other than water uptake, which control the proton conduction in sub- μ m thick, confined ionomer films. Under such circumstances, the decisive factors for proton conduction may be the size and long-range connectivity of water (or ionic) domains

(subject to experimental evidence). Percolated, large water domains, and/or extended hydrogen-bonded water network with sufficient rotational mobility of water⁴¹ are highly required for efficient proton transfer.⁷⁸ If the hydrophilic domains are small, scattered and not-well-connected, proton transfer can be weak no matter how high the water uptake is. We thus investigated the characteristics of ionic domains (domain size, domain spacing, morphology) using RSAXS, bright-field TEM, and fluorescence spectroscopy.

RSAXS Measurement. Figure 6 shows the in-plane RSAXS patterns of annealed ionomer films under ambient conditions (56% RH). Within the scattering vector (q_p) range of $1.50-3.50~\rm nm^{-1}$, a single ionic domain (with no periodicity) was observed for the ionomer films (Figure 6). For all three ionomers, ionic domain peak maxima $(q_{p,max})$ shifted to higher q_p value and decreased in scattering intensity $(I(q_p))$ as the films became thinner (Figure 6 and Table 2). These indicated

Table 2. $(q_p)_{max}$, Full-Width-at-Half-Maxima (FWHM) of Ionic Domain Peak and Domain Spacing (*d*-spacing) of Nafion, 3M PFSA, and 3M PFIA Ionomer Films on SiO₂ from RSAXS Data at Ambient Condition (~56% RH)

		ionic domain				
polymers	sample thickness (nm)	$q_{\rm p \ max} \ ({\rm nm}^{-1})$	full-width at half maxima of ionomer peak (fwhm) (nm ⁻¹)	d-spacing (nm)		
3M PFIA	468	1.54	0.58	4.06		
	237	1.64	0.65	3.84		
	177	1.64	0.77	3.84		
	71	1.72	0.75	3.60		
	50	1.72	0.78	3.55		
	27	1.82	0.78	3.50		
3M PFSA	443	1.99	0.81	3.16		
	350	2.12	0.77	2.97		
	184	2.36	0.85	2.66		
	62	2.38	1.00	2.64		
	41	2.45	1.00	2.57		
	25	no peak	а	a		
Nafion	470	2.16	0.70	2.90		
	251	2.246	0.74	2.81		
	161	2.32	0.88	2.72		
	72	2.35	0.87	2.67		
	41	2.41	1.04	2.61		
	17	no peak	а	a		

 $[^]ad$ -spacing and fwhm could not be calculated for these films since the ionic domain peaks were not present.

a decrease in domain spacing ($d=2\pi/q_{\rm p\ max}$) or close-packing of ionic domains in thinner films. Also, the neighboring ionic domains were the closest (i.e., the shortest d-spacing) for Nafion and the farthest for 3M PFIA films with a similar thickness (Table 2). The ionic domain peaks completely disappeared for both Nafion and 3M PFSA films at thickness down to ~25 nm, while ~27 nm thick 3M PFIA film still retained the ionic domain peak (Figure 6 and Table 2). This supported stronger hydrophilic—hydrophobic phase separation and existence of well-developed ionic domains even in ultrathin films of 3M PFIA at moderate humidity (56% RH here).

Thinner films, with the larger value of fwhm (Table 2), can reasonably be assumed as less-well-ordered 13,79 and/or less correlated systems 13,79,80 as compared to thicker films (with

narrow ionic domains peak and low fwhm). Kusoglu et al.²⁰ also suggested lower fwhm as a sign of low polydispersity of ionic domain size and spacing. Of the three ionomers, 3M PFIA thus had the largest spacing between ionic domains, but the narrowest distribution of ionic domain spacing and size (Table 2). When the humidity was increased from 56% to 90% RH, the ionic domain peak shifted to lower q_p values (dspacing increased) (Figure 7a-d). In the case of 25 nm thick PFSA (Figure 7e) and 20 nm thick Nafion (Figure 7f) films, no ionic domain peak was observed at 56% RH, but small ionic domain peaks evolved at 90% RH. On the other hand, 3M PFIA showed an ionic domain peak at both 56% and 90% RH, irrespective of film thickness. The fwhm values of ionic domain peaks were \sim 0.67, 0.95, and 0.94 nm⁻¹ for \sim 25 nm thick 3M PFIA, 3M PFSA, and Nafion films at 90% RH, respectively. The relatively long, but flexible side chain may have facilitated better phase segregation in 3M PFIA films and led to the narrow distribution of ionic domain spacing and size.

Despite better phase segregation, the long, hydrophobic side chains of 3M PFIA may have suppressed the effect of polar $-\mathrm{SO}_2$ groups and prevented extreme water uptake ($\lambda_\mathrm{w}\sim6.26$ for 25 nm thick PFIA film, measured by us) which did not happen in the case of Nafion ($\lambda_\mathrm{w}\sim18.5$ for 23 nm thick Nafion film¹⁸) with shorter hydrophobic chains and polar perfluoroether groups. The values of d-spacing were 3.80 and 2.90 nm for ~27 nm thick 3M PFIA and Nafion films at 90% RH, respectively. Such close-packing of ionic domains and higher water uptake ($\lambda_\mathrm{w}\sim18.5$) in Nafion films suggested the presence of a large number of small-sized ionic domains (to accommodate the sorbed water) and thus a higher degree of phase mixing which naturally could not facilitate effective proton conduction in Nafion thin films(Figure 4).

Morphology of Ionic Domains (TEM). The bright-field TEM images of dry ionomer films (Figure 8) were taken under a high vacuum, so the morphologies of these films may not necessarily represent those of films at atmospheric pressure (used for RSAXS and fluorescence spectroscopy measurements). However, relative differences in the morphology and ionic domain size among the three ionomer films at comparable thicknesses can be conferred since all the TEM images were taken at similar conditions (under vacuum). Also, the use of SiO₂-based grids as substrates to make films for TEM studies ensured substrate effect similar to RSAXS, fluorescence, and QCM measurements. A decrease in phase separation was anticipated based on the gradually reduced dark and light contrast in the TEM images when the film thickness of 3M PFIA (Figure 8a-c) and 3M PFSA (Figure 8d-f) decreased from ~75 to ~25 nm. Nafion (Figure 8g-i), on the other hand, showed poor contrast, suggesting a higher degree of phase mixing for the entire film thickness range (\sim 25–75 nm). The projected overlap of electron signals in TEM may prevent accurate determination of ionic domain symmetry or size. However, Allen et al.⁸¹ observed spherical domains with diameter \sim 3.5 \pm 0.3 nm for 100 nm thick Nafion membrane (unstained) under bright-field TEM. Even if we do not go for a quantitative comparison of the ionic domains based on TEM, the visual inspection clearly identifies morphological differences between Weber's 81 and our (Figure 8g) Nafion film with similar thicknesses. The morphological differences could be due to the differences in the TEM sample preparation technique as well as substrate effects. The ionomer films in Weber's work⁸¹ were spun on SiO₂ wafer but then floated on water to transfer onto Cu-mesh TEM grids to obtain TEM

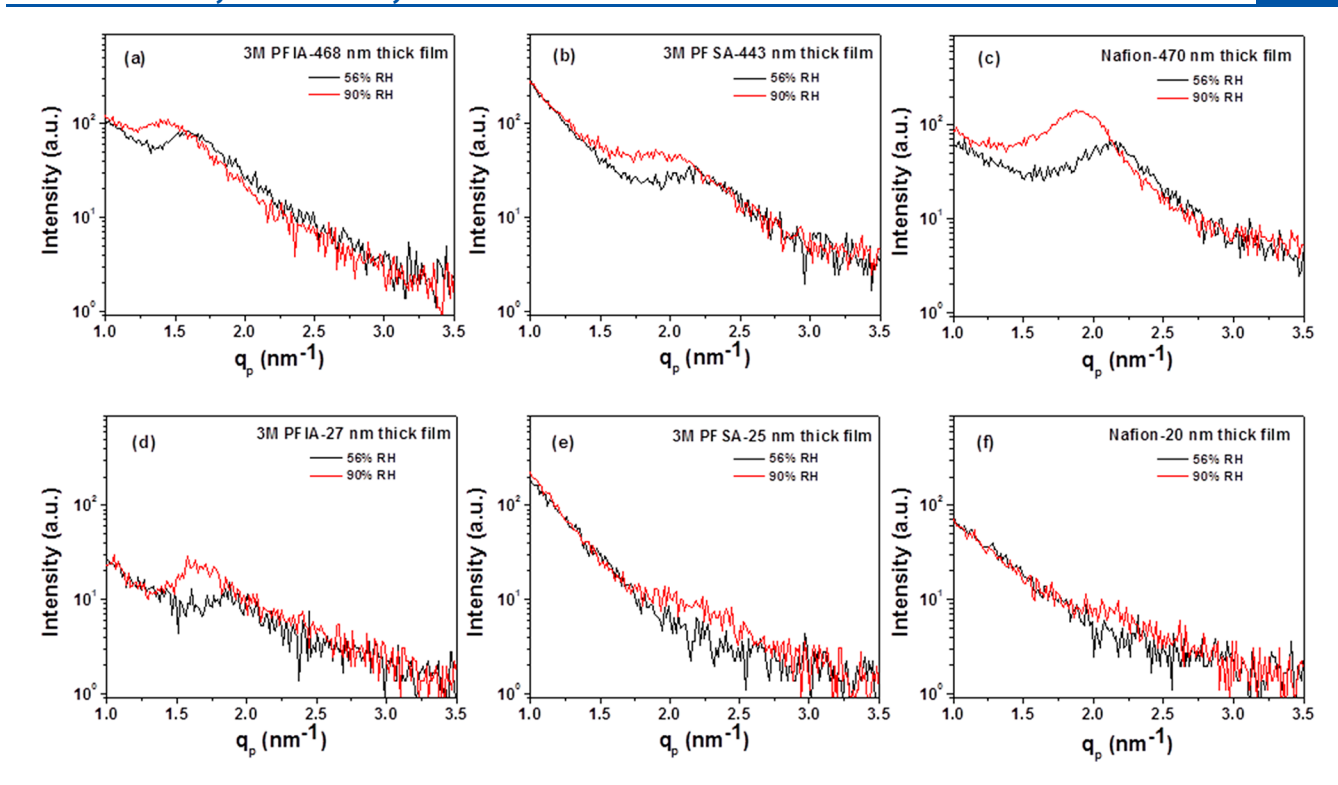


Figure 7. RSAXS profiles of 3M PFIA (a, d), 3M PFSA (b, e), and Nafion (c, f) films on SiO₂ as a function of relative humidity.

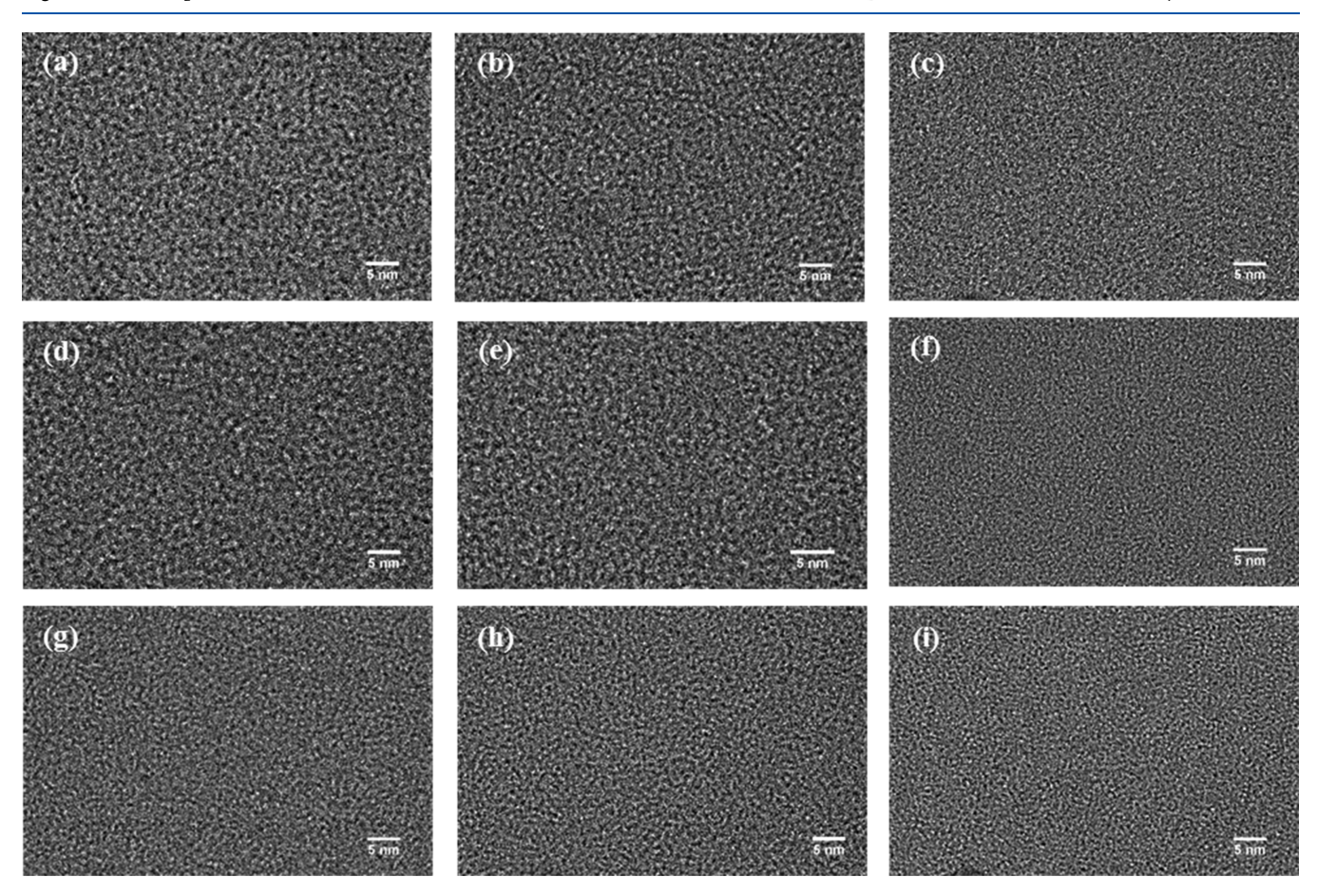


Figure 8. Bright-field TEM images of (a) 75, (b) 40, and (c) 27 nm thick 3M PFIA; (d) 75, (e) 40, and (f) 25 nm thick 3M PFSA; and (g) 72, (h) 41, and (i) 20 nm thick Nafion films spin-coated on 40 nm thick SiO₂ layers. The images were taken under vacuum.

images of unannealed films. On the contrary, we directly spun Nafion films on SiO_2 -based TEM grids and annealed subsequently. Thus, our samples did not undergo the hydration—dehydration cycle (prior to TEM measurements under vacuum) and ion channel formation/structural changes induced by that. 82

Size of Ionic Domains. We utilized RSAXS and steadystate fluorescence techniques independently to predict the average size of ionic domains. While the exact meaning of ionic domain peaks can certainly be a point of debate, an added advantage of fluorocarbon-based ionomers is that a good number of SAXS/GISAXS based, well-accepted models, are available (especially for bulk membrane systems). On the basis of these models, a moderately reasonable argument on the ionic domain geometry/shape in the ionomeric materials studied in this work can be placed. Before proceeding to predict the size of ionic domains in 3M PFIA, 3M PFSA and Nafion thin films, the existing models 13,83,84 on ionomer structures (based on SAXS/GISAXS) were, therefore, carefully reviewed so that our RSAXS data could be interpreted rationally to elucidate ionic domain shape and size in thin films. By far, many different phase-separated structures have been proposed for ionomers, such as networks of interconnected spherical water clusters (Gierke);⁸⁵ core—shell structure;⁸⁶ parallel cylindrical water nanochannels;⁸⁷ rod-like elongated polymer aggregates; ⁸⁸ bicontinuous networks of hydrophilic domains; ^{90,20} Haubold et al. ⁸⁶ proposed a core—shell model for Nafion where the core is either empty (dry state) or filled with water-methanol (wet condition), and, the shell is made of perfluorinated side chains of ionomers with the sulfonic acid groups at the core-shell interface. This structure is similar to reverse micelle systems encapsulating water pools at the core. The complex structure of cross-linked channels was described as a composition of this basic core-shell structure, as per this model.86 Gebel91 proposed the changes in the morphology of hydrated ionomer membranes as a function of water volume fraction (φ_w) . The dry membrane was characterized by isolated spherical ionic clusters. As the water sorption starts, the spherical clusters swell to hold pools of water at the core surrounded by ionic groups (sulfonic acid) at the waterpolymer interface. These spherical domains start to get connected via cylindrical regions made of water molecules (dispersed in a polymer matrix) when $\varphi_{\rm w} \sim 0.3-0.5$.

While all these efforts focused on interpreting ionic domains in bulk membranes, the morphologies of sub- μ m thick ionomer films have not yet been elucidated clearly. One of the very few attempts was on 100 nm thick, unannealed Nafion film⁸¹ using cryo-TEM tomography. The film, however, was hydrated with liquid water (not humid air) and underwent hydration-dehydration cycles during transfer over the TEM grid. Thus, the extended, ribbon-like hydrophilic domains, proposed⁸¹ based on the film prepared this way, may not be relevant to our annealed ionomer films having no prior hydration history. Mobility of water molecules in annealed films is more restricted and thus the connectivity of ionic domains is less obvious. 15,19,23 We then moved back to Gebel's model⁹¹ to explore what morphology this model suggests for our ionomer films at comparable $\varphi_{\rm w}$. The highest $\lambda_{\rm w}$ we achieved was ~5.5 for 161 nm thick Nafion film at 90% RH (Figure 5). The corresponding $\varphi_{\rm w}$ will be ~0.24 based on negligible volume change of mixing reported for fluorocarbon-based ionomer Nafion and water. ^92,22 This $\varphi_{\rm w}$ value, based on Gebel's model, suggests the presence of reverse micelle structures with water-filled, spherical ionic domains at the core with limited connectivity. If the ionic domain connectivity is limited in the bulk membrane at (φ_w) of ~0.24, the probability of having ionic domain connectivity in sub-µm thick films will be even lower (supported by the literature ^{84,93}). Moreover, our thin films were exposed to humid air, not liquid water. This again makes domain connectivity less probable. Thus, making assumptions of (a) core—shell like structure with (b) spherical ion-conducting water domains at the core and (c) limited ionic domain connectivity for the ionomer films seemed reasonable while fitting ionic domain peak of RSAXS data to yield the size of ionic domains in thin films. This assumption was further supported by the recent review by Kusoglu and Weber 13 where the possibility of the existence of isolated spherical ionic domains was not overruled especially at low humidity conditions and if the connectivity of ionic domains is poor (highly likely in confined, thin ionomer film systems 15,94,84,95)

To get the ionic domain size $(d_{\rm id})$ within ionomer films from RSAXS measurements, the ionic domain peaks were fitted using Nanosolver (Rigaku's built-in software with RSAXS system). A core—shell model was chosen (as discussed in the previous section) where (i) the ionic domains containing water and the proton conducting groups of side chains were taken as the core; and (ii) the fluorocarbon ionomer chains were assumed to comprise the shell, respectively. The experimentally obtained values of d-spacing were used as one of the input values (please see Supporting Information and Figure S4 for additional details on fits).

The size of ionic domains (d_{id}) was also predicted using fluorescence data by comparing the $I_{\rm d}/I_{\rm p}$ values of HPTS for ionomer films to that reported for sodium bis (2-ethylhexyl)sulfosuccinate (Aerosol OT or AOT) reverse micelle systems. 12,96 AOT reverse micelles are sulfonated surfactant assemblies which encapsulate nanoscopic water, and have been used frequently as models of confined aqueous environments.¹² The size of polar (or water) pools in AOT reverse micelles has been reported as a function of water-to-AOT mixing ratios (w_0) . At first, we plotted I_d/I_p of HPTS within AOT reverse micelle as a function of the diameter of its hydrophilic core (or water pool, $d_{\rm wp} = 0.29w_0 + 1.11$, with w_0 obtained from the literature (Figure S5)). Then this $I_{\rm d}/I_{\rm p}$ vs $d_{\rm wp}$ plot was used to predict the size of ionic domains (d_{id}) within our ionomer films at certain I_d/I_p . The values of the size of ionic domains in films of all three ionomers, independently obtained from RSAXS and steady-state fluorescence, are presented in Table 3.

In all of the sub-\$\mu\$m thick ionomer films, ionic domains were much smaller (between 1.60 and 2.55 nm) than what was reported for Nafion membranes (\$\sim4\$ nm).\$^{85}\$ Size of ionic domains in sub-\$\mu\$m thick films of 3M PFIA, 3M PFSA, and Nafion is rarely reported except by Allen et al.\$^{81}\$ (discussed earlier in the TEM section). The average diameter of the ionic domains reported by us (\$\sim4\$1.6-2.12 nm) for Nafion thin films (Table 3) is much smaller than what they reported (\$\sim4\$3.5-5 nm). The narrower ionic domains in our samples are logically possible as our films (unlike Allen's ones) were not exposed to liquid water, and did not undergo hydration-dehydration cycles during sample preparation. As shown in Table 3, the average size of ionic domains in 468 nm thick PFIA film was 1.86 nm at 56% RH, and 2.55 nm at 90% RH using RSAXS; however, it was 1.78 nm at 56% RH and 2.55 nm at 90% RH

Table 3. Comparison of Size of Ionic Domains (d_{id})s of 3M PFIA, 3M PFSA, and Nafion Ionomer Films Obtained from RSAXS and Fluorescence Data

		size of the ionic domain $(d_{\mathrm{id}},\mathrm{nm})$				
		RSAXS ^{a,b}		fluorescence ^c		
polymers	sample thickness (nm)	56% RH	90% RH	56% RH	90% RH	
3M PFIA	468	1.86	2.55	1.78	2.55	
3M PFSA	443	1.80	2.10	1.68	2.10	
Nafion	470	1.75	2.12	1.63	1.90	
3M PFIA	27	1.70	1.9-1.95	_	_	
3M PFSA	25	no peak	1.55-1.65	_	_	
Nafion	20	no peak	1.60 - 1.65	_	_	

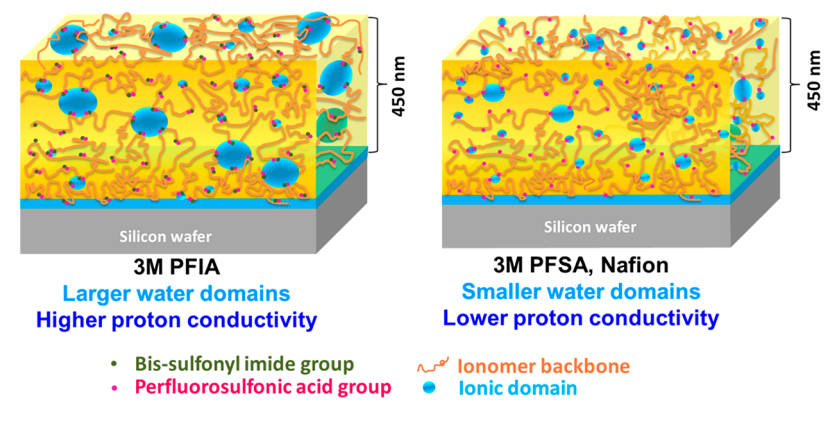
^aThe size of the ionic domains (d_{id}) from in-plane RSAXS was obtained by fitting the ionic domain peak using Nanosolver software. For some of the thinner ionomer films (<30 nm), the no ionic domain peak was observed at ambient conditions. Thus, the size of the ionic domains could not be calculated for those films. ^bFor the size of ionic domains of ~25 nm thick films, a range of size was shown since any value within those ranges can be considered as the best fits. For other films, the single, consistent, repeatable best fit of the peaks was obtained. c Size of ionic domains (d_{id}) from steady-state fluorescence data was obtained by comparing the deprotonation ratio (I_d/I_p) of HPTS in ionomer films to that in sodium bis (2-ethylhexyl) sulfosuccinate (AOT) reverse micelles with the known size of water domains (d_{wp}) . For thinner films (<50 nm), the fluorescence intensities were too low to correctly measure I_d/I_p and predict the size of ionic domains. The values of ionic domain size varied insignificantly (1-2%); therefore, precision error bars were not shown.

using fluorescence. The values closely matched each other. Such agreement of size of ionic domains obtained via RSAXS and fluorescence was observed for all the ionomers in films with ~25 and ~450 nm thickness. This reveals that fluorescence is a reliable technique to quantify the characteristic parameters of ionic domains $(d_{\rm id}, {\rm pH}, I_{\rm d}/I_{\rm p})$ which give rise to quantitative values of proton conductivity (σ) . Most importantly, both the extent of proton conduction $(I_{\rm d}/I_{\rm p}, {\rm Figure } 3, 4)$ and the size of ionic domains $(d_{\rm id}, {\rm Table } 3)$ followed the same trend: 3M PFIA > 3M PFSA > Nafion. It is now evident that water domain size, not the water uptake, dominantly controls proton conduction properties of thin ionomer films (Figure 9).

Larger ionic domains (as seen for 3M PFIA) favored proton conduction (Figure 9, left); and in the formation of ionic domains, ionomer side-chain length, flexibility, and acidity played important roles. The long, flexible⁵³ side chains of ionomers (3M PFIA) may naturally have relatively higher mobility to reach out to the water, facilitate water segregation, and form larger ionic domains (Figure 9, left). The high protogenicity⁵¹ of side-chains of 3M PFIA then acts as an additional feature that favors the proton conduction more in such large water domains. On the other hand, due to short (3M PFSA) and stiff (3M PFSA, Nafion) side chains, 3M PFSA and Nafion form smaller ionic domains (Figure 9, right). A small ionic domain significantly constrains water molecules in taking necessary steps for long-range proton conduction or hopping, such as forming hydrogen-bonded water network and dynamically rotating, relaxing, breaking, and forming hydrogen bonds to conduct the protons to neighboring water molecules.¹² Therefore, 3M PFIA thin films, with relatively larger water pools, conduct proton more efficiently than 3M PFSA and Nafion thin films, with relatively smaller water pools. We also found that the diameter of ionic domains in ionomer films decreased as the film thickness and RH decreased (Table 3). In thinner films (~25 nm thick here), ionomer chains can be confined, and lack enough mobility 15,18 to facilitate efficient phase segregation, and large ionic domain formation (an effect similar to rigid side-chain effect). High water uptake in thinner films ($\lambda_{\rm w} \sim 18.5$ for 23 nm thick Nafion film as opposed to ~5.5 for 470 nm thick Nafion film) may thus lead to a large number of small, ill-connected ionic domains where protons are confined. This is why thinner films exhibited a lower extent of proton conduction (I_d/I_p) as compared to thicker films.

CONCLUSIONS

The critical parameters of hydration environment within sub- $\mu \rm m$ thick films (water uptake $(\lambda_{\rm w})$, ionic domain size $(d_{\rm id})$, pH, the extent of proton conduction $(I_{\rm d}/I_{\rm p}))$ of three fluorocarbon-based ionomers (3M PFIA, 3M PFSA, Nafion) were quantified. Using fluorescent photoacid probe HPTS, it was shown that 3M PFIA has the most favorable proton conduction environment of the three ionomers studied. High hydration $(\lambda_{\rm w})$ did not help to achieve a high extent of proton conduction $(I_{\rm d}/I_{\rm p})$, but the size of the ionic domain $(d_{\rm id})$ did. Using RSAXS and fluorescence spectroscopy, the size of ionic domains within ionomers films was then independently



Not the water uptake, but the size of the water domains matters!

Figure 9. Schematic representation of ionic domain characteristics within thin films of the ionomers studied in this work.

measured. The extent of proton conduction (I_d/I_p) followed the trend similar to the size of ionic domains (3M PFIA > 3M PFSA > Nafion). Also thinner films, despite higher water uptake, showed lower I_d/I_p , and smaller ionic domains. The study suggests that even if the water uptake is high, the extent of proton conduction (I_d/I_p) can be low if the individual water domains in an ionomer film are small and not-connected. The flexibility, hydrophilicity, and multiple acid groups in the side chain of 3M PFIA in thin films allowed the formation of larger ionic domains with better phase separation and facilitated better water-mediated proton conduction. On the contrary, phase segregation and formation of large ionic domains were not facilitated in 3M PFSA and Nafion films due to the short and/or less flexible side-chains of these ionomers. In these small, ill-connected ionic domains, the rotational relaxation of water was restricted. The dissociated protons in Nafion and 3M PFSA films thus accumulated within the ionic domains, created an extremely acidic environment, and failed to conduct. This is why Nafion films showed a lower extent of proton conduction (I_d/I_p) (as compared to 3M PFIA films), despite having a higher water uptake. Similarly thinner films formed from any ionomer that exhibited lower I_d/I_p (as compared to thicker films) due to protonic confinement in small, ill-connected water domains.

ASSOCIATED CONTENT

S Supporting Information

The Supporting Information is available free of charge at https://pubs.acs.org/doi/10.1021/acs.jpcc.9b10015.

Additional experimental details (PDF)

AUTHOR INFORMATION

Corresponding Author

*(S.K.D.) E-mail: sdishari2@unl.edu. Telephone: 402-472-7537.

ORCID

Anandakumar Sarella: 0000-0002-6771-9381 Shudipto K. Dishari: 0000-0003-1679-2332

Notes

The authors declare no competing financial interest.

ACKNOWLEDGMENTS

S.K.D. acknowledges supports from the NSF CAREER Award (NSF-DMR # 1750040), Nebraska EPSCoR First Award (1557417), NASA-Nebraska Space Grant (NNX 15AI09H); University of Nebraska—Lincoln (UNL) core facility grant and start-up fund. S.F thanks Mr. Ehsan Zamani for performing the ellipsometric measurement of films. The research was performed in part (TEM and RSAXS measurements) in the Nebraska Nanoscale Facility: National Nanotechnology Coordinated Infrastructure and the Nebraska Center for Materials and Nanoscience, which are supported by the National Science Foundation under Award ECCS: 1542182, and the Nebraska Research Initiative.

REFERENCES

- (1) Smyda, M. R.; Harvey, S. C. The Entropic Cost of Polymer Confinement. J. Phys. Chem. B 2012, 116, 10928–10934.
- (2) Chen, Y.; Lin, Y.; Chang, J.; Lin, P. Dynamics and Conformation of Semi Flexible Polymers in Strong Quasi-1D and -2D Confinement. *Macromolecules* **2014**, *47*, 1199–1205.

- (3) Chaudhuri, D.; Mulder, B. Size and Shape of Excluded Volume Polymers Confined between Parallel Plates. *Phys. Rev. E* **2011**, 83, 031803.
- (4) O' Connell, P. A.; McKenna, G. B. Rheological Measurements of the Thermoviscoelastic Response of Ultrathin Polymer Films. *Science (Washington, DC, U. S.)* **2005**, 307, 1760–1763.
- (5) Mckenna, G. B. Dynamics of Materials at the Nanoscale: Small-Molecule Liquids and Polymer Films. *Polymer Physics:From Suspensions to Nanocomposites and Beyond* **2010**, 191–223.
- (6) Ellison, C. J.; Kim, S. D.; Hall, D. B.; Torkelson, J. M. Confinement and Processing Effects on Glass Transition Temperature and Physical Aging in Ultrathin Polymer Films: Novel Fluorescence Measurements. *Eur. Phys. J. E: Soft Matter Biol. Phys.* **2002**, *8*, 155–166.
- (7) Ellison, C. J.; Torkelson, J. M. The Distribution of Glass-Transition Temperatures in Nanoscopically Confined Glass Formers. *Nat. Mater.* **2003**, *2*, 695–700.
- (8) Kim, S.; Torkelson, J. M. Distribution of Glass Transition Temperatures in Free-Standing, Nanoconfined Polystyrene Films: A Test of de Gennes' Sliding Motion Mechanism. *Macromolecules* **2011**, 44, 4546–4553.
- (9) Frank, B.; Gast, A. P.; et al. Polymer Mobility in Thin Films. *Macromolecules* **1996**, 29, 6531–6534.
- (10) Miller, K. E.; Krueger, R. H.; Torkelson, J. M. Mobility-Sensitive Fluorescence Probes for Quantitative Monitoring of Water Sorption and Diffusion in Polymer Coatings. *J. Polym. Sci., Part B: Polym. Phys.* **1995**, 33, 2343–2349.
- (11) Fayer, M. D. Dynamics of Water Interacting with Interfaces, Molecules, and Ions. Acc. Chem. Res. 2012, 45, 3-14.
- (12) Fayer, M. D.; Levinger, N. E. Analysis of Water in Confined Geometries and at Interfaces. *Annu. Rev. Anal. Chem.* **2010**, *3*, 89–107.
- (13) Kusoglu, A.; Weber, A. Z. New Insights into Perfluorinated Sulfonic-Acid Ionomers. *Chem. Rev.* **2017**, *117*, 987–1104.
- (14) Holdcroft, S. Fuel Cell Catalyst Layers: A Polymer Science Perspective. *Chem. Mater.* **2014**, *26*, 381–393.
- (15) Dishari, S. K.; Hickner, M. A. Confinement and Proton Transfer in Nafion Thin Films. *Macromolecules* **2013**, *46*, 413–421.
- (16) Siroma, Z.; Kakitsubo, R.; Fujiwara, N.; Ioroi, T.; Yamazaki, S.; Yasuda, K. Depression of Proton Conductivity in Recast Nafion ® Film Measured on Flat Substrate. *J. Power Sources* **2009**, *189*, 994–998.
- (17) Davis, E. M.; Stafford, C. M.; Page, K. A. Elucidating Water Transport Mechanisms in Nafion Thin Films. *ACS Macro Lett.* **2014**, 3, 1029–1035.
- (18) Dishari, S. K.; Hickner, M. A. Antiplasticization and Water Uptake of Nafion® Thin Films. ACS Macro Lett. 2012, 1, 291–295.
- (19) Dishari, S. K.; Rumble, C. A.; Maroncelli, M.; Dura, J. A.; Hickner, M. A. Unraveling the Complex Hydration Behavior of Ionomers under Thin Film Confinement. *J. Phys. Chem. C* **2018**, *122*, 3471–3481.
- (20) Kusoglu, A.; Dursch, T. J.; Weber, A. Z. Nanostructure/ Swelling Relationships of Bulk and Thin-Film PFSA Ionomers. *Adv. Funct. Mater.* **2016**, *26*, 4961–4975.
- (21) Shrivastava, U. N.; Fritzsche, H.; Karan, K. Interfacial and Bulk Water in Ultrathin Films of Nafion, 3M PFSA, and 3M PFIA Ionomers on a Polycrystalline Platinum Surface. *Macromolecules* **2018**, *51*, 9839–9849.
- (22) Kusoglu, A.; Kushner, D.; Paul, D. K.; Karan, K.; Hickner, M. A.; Weber, A. Z. Impact of Substrate and Processing on Confinement of Nafion Thin Films. *Adv. Funct. Mater.* **2014**, *24*, 4763–4774.
- (23) Modestino, M. A.; Paul, D. K.; Dishari, S.; Petrina, S. A.; Allen, F. I.; Hickner, M. A.; Karan, K.; Segalman, R. A.; Weber, A. Z. Self-Assembly and Transport Limitations in Confined Nafion Films. *Macromolecules* **2013**, *46*, 867–873.
- (24) Maldonado, L.; Perrin, J. C.; Dillet, J.; Lottin, O. Characterization of Polymer Electrolyte Nafion Membranes: Influence of Temperature, Heat Treatment and Drying Protocol on Sorption and Transport Properties. J. Membr. Sci. 2012, 389, 43–56.

- (25) Onishi, L. M.; Prausnitz, J. M.; Newman, J. Water-Nafion Equilibria. Absence of Schroeder's Paradox. *J. Phys. Chem. B* **2007**, *111*, 10166–10173.
- (26) Lee, K.; Ishihara, A.; Mitsushima, S.; Kamiya, N.; Ota, K. Effect of Recast Temperature on Diffusion and Dissolution of Oxygen and Morphological Properties in Recast Nafion. *J. Electrochem. Soc.* **2004**, *151*. A639.
- (27) Giffin, G. A.; Haugen, G. M.; Hamrock, S. J.; Di Noto, V. Interplay between Structure and Relaxations in Perfluorosulfonic Acid Proton Conducting Membranes. *J. Am. Chem. Soc.* **2013**, 135, 822–834
- (28) Dura, J. A.; Murthi, V. S.; Hartman, M.; Satija, S. K.; Majkrzak, C. F. Multilamellar Interface Structures in Nafion. *Macromolecules* **2009**, 42, 4769–4774.
- (29) Murthi, V. S.; Dura, J. S.; Satija, S.; Majkrzak, C. F. Water Uptake and Interfacial Structural Changes of Thin Film Nafion(R) Membranes Measured by Neutroon Reflectivity for PEM Fuel Cells. ECS Transac. 2008, 16, 1471–1485.
- (30) Paul, D. K.; Karan, K. Conductivity and Wettability Changes of Ultrathin Nafion Films Subjected to Thermal Annealing and Liquid Water Exposure. *J. Phys. Chem. C* **2014**, *118*, 1828–1835.
- (31) Dishari, S. K. Current Understanding of Proton Conduction in Confined Ionomeric Systems. *PostDoc J.* **2014**, *2*, 30–39.
- (32) Choi, P.; Jalani, N. H.; Datta, R. Thermodynamics and Proton Transport in Nafion. *J. Electrochem. Soc.* **2005**, *152*, E123–E130.
- (33) Xu, K.; Oh, H.; Hickner, M. A.; Wang, Q. Highly Conductive Aromatic Ionomers with Perfluorosulfonic Acid Side Chains for Elevated Temperature Fuel Cells. *Macromolecules* **2011**, *44*, 4605–4609.
- (34) Rubatat, L.; Rollet, A. L.; Gebel, G.; Diat, O. Evidence of Elongated Polymeric Aggregates in Nafion. *Macromolecules* **2002**, *35*, 4050–4055.
- (35) Kreuer, K. D. On the Development of Proton Conducting Polymer Membranes for Hydrogen and Methanol Fuel Cells. *J. Membr. Sci.* **2001**, *185*, 29–39.
- (36) Paul, D. K.; Fraser, A.; Karan, K. Towards the Understanding of Proton Conduction Mechanism in PEMFC Catalyst Layer: Conductivity of Adsorbed Nafion Films. *Electrochem. Commun.* **2011**, *13*, 774–777.
- (37) Decaluwe, S. C.; Baker, A. M.; Bhargava, P.; Fischer, J. E.; Dura, J. A. Structure-Property Relationships at Nafion Thin-Film Interfaces: Thickness Effects on Hydration and Anisotropic Ion Transport. *Nano Energy* **2018**, *46*, 91–100.
- (38) Decaluwe, S. C.; Kienzle, P. A.; Bhargava, P.; Baker, A. M.; Dura, J. A. Phase Segregation of Sulfonate Groups in Nafion Interface Lamellae, Quantified via Neutron Reflectometry Fitting Techniques for Multilayers Structures. *Soft Matter* **2014**, *10*, 5763–5776.
- (39) Spry, D. B.; Goun, A.; Glusac, K.; Moilanen, D. E.; Fayer, M. D. Proton Transport and the Water Environment in Nafion Fuel Cell Membranes and AOT Reverse Micelles. *J. Am. Chem. Soc.* **2007**, *129*, 8122–8130.
- (40) Baker, J. M.; Dore, J. C.; Seddon, J. M.; Soper, A. K. Structural Modification of Water in the Confined Layer of a Lamellar Lipid Crystal. *Chem. Phys. Lett.* **1996**, 256, 649–652.
- (41) Laage, D. A Molecular Jump Mechanism of Water Reorientation. Science (Washington, DC, U. S.) 2006, 311, 832-835.
- (42) Moilanen, D. E.; Spry, D. B.; Fayer, M. D. Water Dynamics and Proton Transfer in Nafion Fuel Cell Membranes. *Langmuir* **2008**, *24*, 3690–3698.
- (43) Tesfaye, M.; Macdonald, A. N.; Dudenas, P. J.; Kusoglu, A.; Weber, A. Z. Exploring Substrate/Ionomer Interaction under Oxidizing and Reducing Environments. *Electrochem. Commun.* **2018**, 87, 86–90.
- (44) Astill, T.; Xie, Z.; Shi, Z.; Navessin, T.; Holdcroft, S. Factors Influencing Electrochemical Properties and Performance of Hydrocarbon-Based Electrolyte PEMFC Catalyst Layers. *J. Electrochem. Soc.* **2009**, *156*, B499–B508.

- (45) Yandrasits, M.; Lindell, M.; Schaberg, M.; Kurkowski, M. Increasing Fuel Cell Efficiency by Using Ultra-Low Equivalent Weight Ionomers. *Electrochem. Soc. Interface* **2017**, *26*, 49–53.
- (46) Miyake, J.; Taki, R.; Mochizuki, T.; Shimizu, R.; Akiyama, R.; Uchida, M.; Miyatake, K. Design of Flexible Polyphenylene Proton-Conducting Membrane for next-Generation Fuel Cells. *Sci. Adv.* **2017**, 3, eaao0476.
- (47) Chang, Y.; Brunello, G. F.; Fuller, J.; Disabb-Miller, M. L.; Hawley, M. E.; Kim, Y. S.; Hickner, M. A.; Jang, S. S.; Bae, C. Polymer Electrolyte Membranes Based on Poly(Arylene Ether Sulfone) with Pendant Perfluorosulfonic Acid. *Polym. Chem.* **2013**, *4*, 272–281.
- (48) Hickner, M. A.; Ghassemi, H.; Kim, Y. S.; Einsla, B. R.; Mcgrath, J. E. Alternative Polymer Systems for Proton Exchange Membranes (PEMs). *Chem. Rev.* **2004**, *104*, 4587–4612.
- (49) Economou, N. J.; Barnes, A. M.; Wheat, A. J.; Schaberg, M. S.; Hamrock, S. J.; Buratto, S. K. Investigation of Humidity Dependent Surface Morphology and Proton Conduction in Multi-Acid Side Chain Membranes by Conductive Probe Atomic Force Microscopy. *J. Phys. Chem. B* **2015**, *119*, 14280–14287.
- (50) Liu, Y.; Horan, J. L.; Schlichting, G. J.; Caire, B. R.; Liberatore, M. W.; Hamrock, S. J.; Haugen, G. M.; Yandrasits, M. A.; Seifert, S.; Herring, A. M. A Small-Angle X-ray Scattering Study of the Development of Morphology in Films Formed from the 3M Perfluorinated Sulfonic Acid Ionomer. *Macromolecules* **2012**, *45*, 7495–7503.
- (51) Atrazhev, V. V.; Astakhova, T. Y.; Sultanov, V. I.; Perry, M. L.; Burlatsky, S. F. Molecular Dynamic Study of Water-Cluster Structure in PFSA and PFIA Ionomers. *J. Electrochem. Soc.* **2017**, *164*, F1265–F1271.
- (52) Sumner, J. J.; Creager, S. E.; Ma, J. J.; DesMarteau, D. D. Proton Conductivity in Nafion 117 and in a Novel Bis-[(Perfluoroalkyl)Sulfonyl]Imide Ionomer Membrane. *J. Electrochem. Soc.* 1998, 145, 107.
- (53) Clark, J. K., II; Paddison, S. J. Proton Dissociation and Transfer in Proton Exchange Membrane Ionomers with Multiple and Distinct Pendant Acid Groups: An Ab Initio Study. *Electrochim. Acta* **2013**, 101, 279–292.
- (54) Emery, M.; Frey, M.; Guerra, M.; Haugen, G.; Hintzer, K.; Lochhaas, H.; Pham, P.; Pierpont, D.; Schaberg, M.; Thaler, A.; et al. The Development of New Membranes for Proton Exchange Membrane Fuel Cells. *ECS Trans.* **2007**, *11*, 3–14.
- (55) Mundra, M. K.; Donthu, S. K.; Dravid, V. P.; Torkelson, J. M. Effect of Spatial Confinement on the Glass-Transition Temperature of Patterned Polymer Nanostructures. *Nano Lett.* **2007**, *7*, 713–718.
- (56) Huang, Y.; Paul, D. R. Effect of Molecular Weight and Temperature on Physical Aging of Thin Glassy Poly(2,6-Dimethyl-1,4-Phenylene Oxide) Films. *J. Polym. Sci., Part B: Polym. Phys.* **2007**, 45, 1390–1398.
- (57) Ellison, C. J.; Miller, K. E.; Torkelson, J. M. In Situ Monitoring of Sorption and Drying of Polymer Films and Coatings: Self-Referencing, Nearly Temperature-Independent Fluorescence Sensors. *Polymer* **2004**, 45, 2623–2632.
- (58) Goodelle, J. P.; Pearson, R. A.; Santore, M. M. Water-Uptake Kinetics in Poly(Methyl Methacrylate) Films with a Fluorescent Rotor Probe. *J. Appl. Polym. Sci.* **2002**, *86*, 2463–2471.
- (59) Priestley, R. D.; Broadbelt, L. J.; Torkelson, J. M. Physical Aging of Ultrathin Polymer Films above and below the Bulk Glass Transition Temperature: Effects of Attractive vs Neutral Polymer-Substrate Interactions Measured by Fluorescence. *Macromolecules* **2005**, *38*, 654–657.
- (60) Priestley, R. D. Structural Relaxation of Polymer Glasses at Surfaces, Interfaces, and In Between. *Science (Washington, DC, U. S.)* **2005**, 309, 456–459.
- (61) Spry, D. B.; Fayer, M. D. Proton Transfer and Proton Concentrations in Protonated Nafion Fuel Cell Membranes. *J. Phys. Chem. B* **2009**, *113*, 10210–10221.
- (62) Lawler, C.; Fayer, M. D. Proton Transfer in Ionic and Neutral Reverse Micelles. J. Phys. Chem. B 2015, 119, 6024–6034.

- (63) Mondal, T.; Das, A. K.; Sasmal, D. K.; Bhattacharyya, K. Excited State Proton Transfer in Ionic Liquid Mixed Micelles. *J. Phys. Chem. B* **2010**, *114*, 13136–13142.
- (64) Han, J.; Burgess, K. Fluorescent Indicators for Intracellular PH-ACS Review.Pdf. Chem. Rev. 2010, 110, 2709–2728.
- (65) Wright, K. M.; Oparka, K. J. The Fluorescent Probe HPTS as a Phloem-Mobile, Symplastic Tracer: An Evaluation Using Confocal Laser Scanning Microscopy. *J. Exp. Bot.* **1996**, *47*, 439–445.
- (66) Zawodzinski, T. A. A Comparative Study of Water Uptake By and Transport Through Ionomeric Fuel Cell Membranes. *J. Electrochem. Soc.* **1993**, *140*, 1981.
- (67) Particle-/Pore-Size Analysis Software NANO-Solver 3.7 User Manual (Basic): Rigaki Corporation.
- (68) Hallik, A.; Roosalu, K.; Mändar, H.; Joosu, L.; Marandi, M.; Tamm, J. Thickness Dependence of the Porosity of PPy/DDS Films. *Eur. Polym. J.* **2015**, *70*, 118–124.
- (69) Shim, H. K.; Paul, D. K.; Karan, K. Resolving the Contradiction between Anomalously High Water Uptake and Low Conductivity of Nanothin Nafion Films on SiO2 Substrate. *Macromolecules* **2015**, *48*, 8394–8397.
- (70) Kobayashi, Y.; Zheng, W.; Chang, T. B.; Hirata, K.; Suzuki, R.; Ohdaira, T.; Ito, K. Nanoporous Structure of Sputter-Deposited Silicon Oxide Films Characterized by Positronium Annihilation Spectroscopy. *J. Appl. Phys.* **2002**, *91*, 1704–1706.
- (71) Kushner, D. I.; Hickner, M. A. Water Sorption in Electron-Beam Evaporated SiO2 on QCM Crystals and Its Influence on Polymer Thin Film Hydration Measurements. *Langmuir* **2017**, 33, 5261–5268.
- (72) Tao, T. Technical Articles. An Epsilon of Room, II 2011, 27, 141-239.
- (73) Ito, Y. Grazing-Incidence Small-Angle X-Ray Scattering Technique for Nanostructure Determination of Surfaces and Interfaces of Thin Films. *Rigaku J.* **2009**, *25*, 1–6.
- (74) Muller-Buschbaum, P. Chapter 3: A Basic Introduction to Grazing Incidence Small-Angle X-Ray Scattering. *Lect. Notes Phys.* **2009**, 776, 61–89.
- (75) Lakowicz, J. R. Principles of Fluorescence Spectroscopy; 2010.
- (76) Koppel, I. A.; Taft, R. W.; Anvia, F.; Zhu, S. Z.; Hu, L. Q.; Sung, K.; Sen; DesMarteau, D. D.; Yagupolskii, L. M.; Yagupolskii, Y. L.; Ignat'ev, N. V.; et al. The Gas-Phase Acidities of Very Strong Neutral Brønsted Acids. J. Am. Chem. Soc. 1994, 116, 3047–3057.
- (77) Paddison, S. J.; Elliott, J. A. On the Consequences of Side Chain Flexibility and Backbone Conformation on Hydration and Proton Dissociation in Perfluorosulfonic Acid Membranes. *Phys. Chem. Chem. Phys.* **2006**, *8*, 2193–2203.
- (78) Ueki, T.; Watanabe, M. Macromolecules in Ionic Liquids: Progress, Challenges, and Opportunities. *Macromolecules* **2008**, *41*, 3739–3749.
- (79) Eastman, S. A.; Kim, S.; Page, K. A.; Rowe, B. W.; Kang, S.; Soles, C. L.; Yager, K. G. Effect of Confinement on Structure, Water Solubility, and Water Transport in Nafion Thin Films. *Macromolecules* **2012**, *45*, 7920–7930.
- (80) Sorte, E. G.; Paren, B. A.; Rodriguez, C. G.; Fujimoto, C.; Poirier, C.; Abbott, L. J.; Lynd, N. A.; Winey, K. I.; Frischknecht, A. L.; Alam, T. M. Impact of Hydration and Sulfonation on the Morphology and Ionic Conductivity of Sulfonated Poly(Phenylene) Proton Exchange Membranes. *Macromolecules* **2019**, *52*, 857–876.
- (81) Allen, F. I.; Comolli, L. R.; Kusoglu, A.; Modestino, M. A.; Minor, A. M.; Weber, A. Z. Morphology of Hydrated As-Cast Nafion Revealed through Cryo Electron Tomography. *ACS Macro Lett.* **2015**, *4*, 1–5.
- (82) Kunimatsu, K.; Bae, B.; Miyatake, K.; Uchida, H.; Watanabe, M. ATR-FTIR Study of Water in Nafion Membrane Combined with Proton Conductivity Measurements during Hydration/Dehydration Cycle. *J. Phys. Chem. B* **2011**, *115*, 4315–4321.
- (83) Mauritz, K. A.; Moore, R. B. State of Understanding of Nafion. *Chem. Rev.* **2004**, *104*, 4535–4585.

- (84) Barnes, A. M.; Buratto, S. K. Imaging Channel Connectivity in Nafion Using Electrostatic Force Microscopy. *J. Phys. Chem. B* **2018**, 122, 1289–1295.
- (85) Hsu, W. Y.; Gierke, T. D. Ion Transport and Clustering in Nafion Perfluorinated Membranes. *J. Membr. Sci.* **1983**, *13*, 307–326. (86) Haubold, H.; Vad, T.; Jungbluth, H.; Hiller, P. Nano Structure of NAFION: A SAXS Study. *Electrochim. Acta* **2001**, *46*, 1559–1563.
- (87) Schmidt-Rohr, K.; Chen, Q. Parallel Cylindrical Water Nanochannels in Nafion Fuel-Cell Membranes. *Nat. Mater.* **2008**, *7*, 75–83.
- (88) Loppinet, B.; Gebel, G. Rodlike Colloidal Structure of Short Pendant Chain Perfluorinated Ionomer Solutions. *Langmuir* **1998**, *14*, 1977–1983.
- (89) Elliott, J. A.; Wu, D.; Paddison, J.; Moore, R. B. A Unified Morphological Description of Nafion Membranes from SAXS and Mesoscale Simulations. *Soft Matter* **2011**, *7*, 6820–6827.
- (90) Kreuer, K.; Portale, G. A Critical Revision of the Nano-Morphology of Proton Conducting Ionomers and Polyelectrolytes for Fuel Cell Applications. *Adv. Funct. Mater.* **2013**, *23*, 5390–5397.
- (91) Gebel, G. Structural Evolution of Water Swollen Perfluorosulfonated Ionomers from Dry Membrane to Solution. *Polymer* **2000**, *41*, 5829–5838.
- (92) Wu, X.; Wang, X.; He, G.; Benziger, J. Differences in Water Sorption and Proton Conductivity between Nafion and SPEEK. J. Polym. Sci., Part B: Polym. Phys. 2011, 49, 1437–1445.
- (93) Nadermann, N. K.; Davis, E. M.; Page, K. A.; Stafford, C. M.; Chan, E. P. Using Indentation to Quantify Transport Properties of Nanophase-Segregated Polymer Thin Films. *Adv. Mater.* **2015**, 27, 4924–4930.
- (94) Ohira, A.; Kuroda, S.; Mohamed, H. F. M.; Tavernier, B. Effect of Interface on Surface Morphology and Proton Conduction of Polymer Electrolyte Thin Films. *Phys. Chem. Chem. Phys.* **2013**, *15*, 11494.
- (95) Paul, D. K.; Mccreery, R.; Karan, K. Proton Transport Property in Supported Nafion Nanothin Films by Electrochemical Impedance Spectroscopy. *J. Electrochem. Soc.* **2014**, *161*, F1395–F1402.
- (96) Kinugasa, T.; Kondo, A.; Nishimura, S.; Miyauchi, Y.; Nishii, Y.; Watanabe, K.; Takeuchi, H. Estimation for Size of Reverse Micelles Formed by AOT and SDEHP Based on Viscosity Measurement. *Colloids Surf., A* **2002**, 204, 193–199.